

Petrogenetic significance of zoned allanite in garnet amphibolites from a paleo-subduction zone: Catalina Schist, southern California

SORENA S. SORENSEN

Department of Mineral Sciences, NHB-119, National Museum of Natural History,
Smithsonian Institution, Washington, DC 20560, U.S.A.

ABSTRACT

Zoned allanite is a minor mineral in highly altered blocks of garnet amphibolite that occur in a metaultramafic melange matrix in the amphibolite unit of the Catalina Schist, southern California. Blocks and matrix alike were affected by a high-*T*, relatively high-*P* hydrothermal event, which locally induced partial melting of blocks and apparently was accompanied by considerable trace element metasomatism. In blocks that show evidence for light rare earth element (LREE) enrichment, allanite contains almost all of the LREE in the rock. Most of such blocks are also migmatitic, but some are not.

Allanite from four LREE-enriched samples that have different whole-rock REE abundances and fractionations was analyzed with the electron microprobe. Three of the samples are migmatites, and one shows no evidence for partial melting. The analyses were obtained for empirically defined zones of uniform brightness in backscattered electron images from the scanning electron microscope (SEM). The zoned allanite displays large ranges of anticorrelated Ca and LREE contents. Variations of these elements and of Al, Cr, Sr, Fe, Mg, and Mn within zoned grains indicate a fairly continuous nature for many substitutions of M^{2+} and M^{3+} cations in allanite. Allanite exhibits two shapes of LREE patterns in the same abundance range. Within single grains, some zones display LREE patterns that are strongly fractionated with respect to adjacent zones. In migmatites, the zones most enriched in REE are not grain cores.

The apparent reverse zoning of allanite in migmatites suggests that LREE were added to the rock volume from an external source during allanite growth. Metamorphic textures and petrologic considerations indicate that at least some of the growth of allanite in migmatites predates the partial melting event. The variations of LREE within grains and between samples may in part reflect local, time-dependent changes of fluid compositions in the subduction-related, hydrothermal and metasomatic system the rocks represent.

INTRODUCTION

The zoning of LREE in allanite ($(Ca, Mn, Ce, La, Y, Th)_2(Fe^{3+}, Fe^{2+}, Ti)(Al, Fe^{3+})_2Si_3O_{12}(OH)$ (Deer et al., 1986) has been used as a petrogenetic indicator of crystallization in granitic magmas (Gromet and Silver, 1983; Sawka et al., 1984; Sawka, 1988). Zoning of REE in allanite has also provided evidence for REE transport and the scale of REE mobility in late-stage hydrothermal fluids derived from such magmas (Exley, 1980). Exley (1980) concluded that zoned allanite in hydrothermal veins from Skye crystallized from fluids and that LREE may have been transported for some distance by hydrothermal fluids of meteoric origin.

The existence, scale, and nature of hydrothermal regimes in subduction zones bear on the thermal evolution and geochemical cycles in convergent margins (Anderson et al., 1976; Anderson et al., 1978; Delany and Helgeson, 1978; Boulégue et al., 1987; Reck, 1987; Peacock, 1987a, 1987b; Bebout and Barton, 1989). Evidence for the action of fluids at moderate- to high-*P*, high-*T* conditions in paleo-subduction zones is found in veined, metasoma-

tized, and hydrated eclogites and garnet amphibolites of subduction complexes (Sorensen, 1988; Sorensen and Grossman, 1989; Philippot and Selverstone, 1989a, 1989b; Franz et al., 1989).

Isolated blocks of garnet amphibolite that are variably altered occur in a melange matrix of metaultramafic rocks in the amphibolite unit of the Catalina Schist, a subduction complex of southern California. These rocks were affected by a relatively high-*T*, moderate- to high-*P* hydrothermal-metasomatic event during Cretaceous subduction zone metamorphism (Mattinson, 1986; Sorensen and Barton, 1987; Sorensen, 1988; Bebout and Barton, 1989; Sorensen and Grossman, 1989). Some garnet amphibolite blocks are enriched in a variety of trace elements, including LREE, with respect to what appear to be less altered blocks and with respect to probable metabasalt protoliths (Sorensen and Grossman, 1989; also see below). Nearly all of the LREE in the former rocks reside in strongly zoned allanite (Sorensen and Grossman, 1989; also see below).

This paper discusses (1) the zoning patterns, textural

relationships, mineral chemistry, and LREE compositions of Catalina allanite and (2) the petrogenetic implications of these data for the geochemical evolution of the garnet amphibolite blocks.

METAMORPHISM AND METASOMATISM IN THE CATALINA AMPHIBOLITE UNIT

The Catalina Schist is a subduction zone metamorphic terrane of probable Cretaceous age, exposed on Santa Catalina Island off the coast of southern California (Suppe and Armstrong, 1972; Platt, 1975, 1976; Mattinson, 1986). The terrane consists of three tectonic units; a structurally low blueschist-facies unit is overlain in turn by a high-*P* greenschist-facies unit and a structurally highest amphibolite-facies unit (Platt, 1975, 1976). The disposition of these units in an inverted metamorphic gradient and their similar K-Ar ages led Platt (1975, 1976) and Peacock (1987a) to conclude that the Catalina Schist represents a tectonothermal regime characteristic of the initiation of subduction.

The upper part of the Catalina amphibolite unit consists of garnet amphibolite blocks in a melange matrix of metaultramafic rocks. This melange probably represents slab-derived material accreted to the mantle wedge, or a portion of the slab-mantle wedge contact of a nascent paleo-subduction zone, or both (Platt, 1975, 1976). The complex was altered and hydrated at conditions of $P = 8\text{--}11$ kbar, $T = 640\text{--}750$ °C (Sorensen and Barton, 1987; Sorensen, 1988).

Hydration and metasomatic effects include (1) nonisochemical amphibolitization of garnet + clinopyroxene-bearing rocks; (2) the convergence of $\delta^{18}\text{O}$ values for mafic and ultramafic rocks to those of waters calculated to be in equilibrium with metasedimentary rocks; (3) formation of high-*T*, silica-enriched ($\text{SiO}_2 \sim 50$ wt%, $\text{MgO} \sim 30$ wt%), and hydrated metaultramafic rocks (containing orthoamphibole, clinoamphibole, or both along with chlorite and talc) in the melange matrix; (4) formation of Si- and Mg-rich rinds (containing orthoamphibole, clinoamphibole, or both and layer silicates) around garnet amphibolite blocks via fluid-mediated exchange between blocks and matrix; (5) trace element enrichment of some garnet amphibolite blocks (Sorensen and Barton, 1987; Sorensen, 1988; Bebout and Barton, 1989; Sorensen and Grossman, 1989). Migmatization of some garnet amphibolite blocks was probably a H_2O -saturated partial melting event (Sorensen and Barton, 1987; Sorensen, 1988; Bertasi and Barton, 1989).

In order of increasing alteration from a probable metabasalt protolith, common types of garnet amphibolite blocks are: (I) nonmigmatitic, clinopyroxene-bearing blocks; (II) nonmigmatitic blocks that are surrounded by rinds of amphibole + layer silicates; (IIIa) migmatitic blocks; and (IIIb) phengite-veined, nonmigmatitic blocks. The highly altered blocks (IIIa, IIIb) contain allanite. Field descriptions and petrologic and geochemical data for the first three groups are presented in Sorensen (1988) and Sorensen and Grossman (1989).

Some trace element metasomatism of the mafic blocks evidently occurred without partial melting (Sorensen and Grossman, 1989). Mass balance calculations based on the whole-rock major and trace element geochemistry of nonmigmatitic, clinopyroxene-bearing blocks suggest that these rocks lack an albite component in contrast to midocean ridge basalts (MORB) (Sorensen, 1988; Sorensen and Grossman, 1989). Nonmigmatitic, rind-bearing garnet amphibolite blocks are uniformly enriched in 10–15% of a peridotite component (including Cr and Ni) compared to the rindless clinopyroxene-bearing blocks (Sorensen, 1988; Sorensen and Grossman, 1989). Some rind-bearing blocks are also modestly enriched in Th, Ta, Nb, P, and LREE. In other metamorphic terranes, amphibole + layer silicate selvages and rinds between mafic to felsic and ultramafic rocks are interpreted to form by fluid-mediated reaction and chemical exchange across contacts (Coleman, 1961, 1967; Curtis and Brown, 1969, 1971; Sanford, 1982; Moore, 1984). In many cases, trace element values for phengite-veined, nonmigmatitic garnet amphibolite blocks (Appendix I, Fig. 1) lie between those of clinopyroxene-bearing blocks and migmatitic blocks. This trace element signature and the major element compositions (Appendix I) of the phengite-veined blocks suggest that they are somewhat altered from a basaltic protolith.

Sorensen and Grossman (1989) analyzed whole rocks and mineral separates from a suite of nonmigmatitic, clinopyroxene-bearing blocks and a suite of migmatites and performed mass balance calculations for a number of trace elements. They concluded that most of the Th, high field strength elements (HFSE), and REE in the rocks reside in the accessory minerals rutile, sphene, garnet, apatite, zircon, zoisite, and (in migmatites) allanite. Several minerals appear to fractionate elements differently in the two rock types. For example, Ta is systematically enriched with respect to Ti in rutile and sphene from migmatites, compared to counterparts in nonmigmatitic blocks. In migmatites, both minerals show evidence for an extended period of crystallization, including a relatively late stage. For instance, veins of rutile grains, up to 2 cm long and bearing fluid inclusions, occur in the migmatite block from which sample MM was obtained; poikiloblastic sphene in the matrix of this block contains inclusions of garnet and amphibole. In the nonmigmatitic, clinopyroxene-bearing blocks, sphene contains most of the U, Th, and LREE in the rock; in contrast, sphene from sample MM contains less Th and La than the whole rock from which it was taken (Sorensen and Grossman, 1989). The average Ce/Th ratio of migmatites is controlled by allanite (Sorensen and Grossman, 1989, Fig. 8b), which suggests both of these elements reside primarily in allanite.

MINERAL ASSEMBLAGES AND WHOLE-ROCK MINOR AND TRACE ELEMENT GEOCHEMISTRY OF THE SAMPLES STUDIED

Allanite grains from samples taken from migmatitic blocks (samples MM, BCM, and 712841) and from a phengite-veined, nonmigmatitic block (sample 41865)

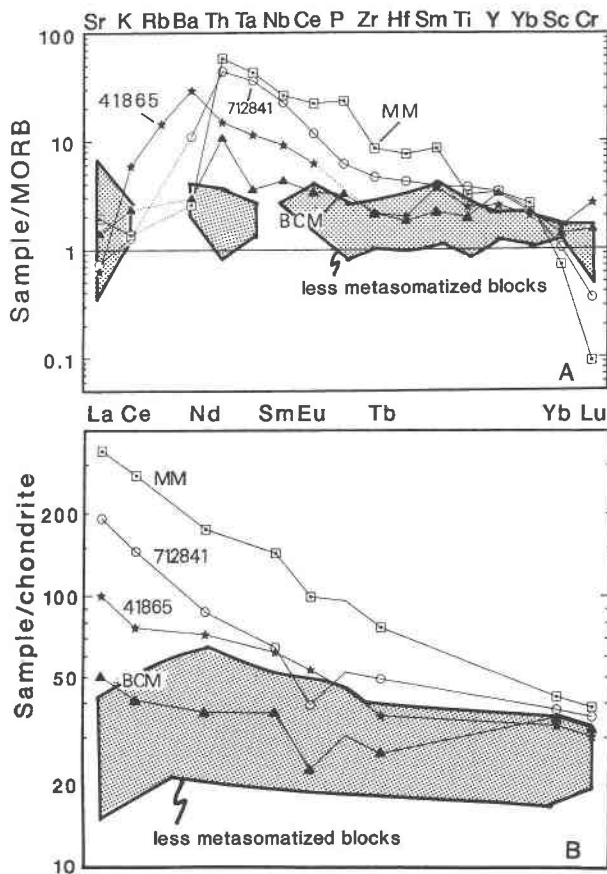


Fig. 1. Minor and trace element abundances (A) and REE abundances (B) of garnet amphibolites. Shaded regions represent the range of values for clinopyroxene-bearing garnet amphibolites (relatively less metasomatized) from the mafic and ultramafic complex of the Catalina amphibolite unit (Sorensen and Grossman, 1989). Values for MORB used for normalization are from Pearce (1982); REE abundances in chondrite are those reported by Anders and Ebihara (1982). Symbols are: open circles = 712841, squares = MM, filled stars = 41865, filled triangles = BCM.

were studied. These samples span the range of LREE compositions of migmatitic blocks reported by Sorensen and Grossman (1989). Petrographic and field descriptions of migmatites are presented in Sorensen (1988) and Sorensen and Grossman (1989). The migmatite samples studied here contain garnet + hornblende + (>2 modal%) plagioclase + (>2 modal%) quartz + (minor) zoisite, clinozoisite, allanite, rutile, zircon, and apatite \pm muscovite \pm (minor) sphene, and chlorite. These samples lack clinopyroxene. Saussuritized plagioclase (An_{02-20}) + quartz \pm muscovite locally comprise podiform leucocratic regions or veins within the samples, or both.

Phengite-veined blocks contain garnet + hornblende + phengitic muscovite + rutile + apatite + allanite + zircon + sphene + chlorite. The crude gneissic foliation of these rocks is locally crosscut by coarse-grained (0.1 to >1 cm grain lengths) anastomosing seams (veins) of phengite (Si

~ 3.3 , Na ~ 0.1 cations per 11 O atoms; Sorensen, 1989). Phengite grains commonly contain inclusions of garnet, hornblende, rutile, zircon, and allanite. The veins probably formed relatively late in the crystallization of the rock from an alkali-rich fluid at high- T , moderate- to high- P conditions. Conventional K-Ar ages for these phengites (106.2 ± 1.7 m.y.) resemble those for phengitic muscovite from leucocratic regions in the migmatites (104.4 ± 1.7 m.y.; K-Ar data from F. MacDowell, personal communication, 1987, 1989).

Analyses of the three migmatites studied are reported in Sorensen and Grossman (1989); the analysis of phengite-veined sample 41865 is reported in Appendix I. Details of the methods (INAA and XRF) by which these samples were analyzed and a discussion of the major, minor, and trace element chemistry of migmatites appear in Sorensen (1988) and Sorensen and Grossman (1989). Migmatite samples 712841 and MM are enriched in Th, high field strength elements (HFSE: Zr, Hf, Ti, Ta, and Nb) and in LREE compared to clinopyroxene-bearing blocks and MORB (Fig. 1). Samples MM and 712841 display more highly fractionated LREE patterns than samples 41865 and BCM (Fig. 1B). With the exception of Th, values for most trace elements in migmatite BCM are similar to, or only slightly greater than, those of the clinopyroxene-bearing blocks (Fig. 1A). However, the weakly LREE-enriched pattern of sample BCM differs from those of the LREE-depleted, clinopyroxene-bearing blocks (Fig. 1B). The phengite-veined sample 41865 is enriched in Th, Ta, Nb, and Ce compared to clinopyroxene-bearing blocks; however, values for these elements range between those for migmatites 712841 and MM and those for migmatite BCM (Fig. 1). The minor and trace element geochemistry of sample 41865 (Fig. 1; also, compare Appendix I to migmatite analyses in Table 1 of Sorensen and Grossman, 1989) resembles that of the migmatites, with the exception that the sample is relatively alkali-rich (Fig. 1A). Sample 41865, like all phengite-veined samples, lacks the distinctive leucocratic regions of the migmatites and shows no other evidence of partial melting.

ANALYTICAL METHODS

Allanite was studied by backscattered electron imaging with a JEOL 840-A SEM, and analyzed (Table 1) with an ARL-SEM-Q electron microprobe in the Department of Mineral Sciences, National Museum of Natural History (NMNH), Smithsonian Institution, Washington, DC. Backscattered electron imaging reveals complex patterns of zones of differing average Z within grains (Figs. 2A–2D). Four to six brightness zones, each with fairly uniform apparent average Z, were empirically defined for each sample by visual inspection of gray-level brightness and by energy dispersive X-ray analysis with the SEM (Figs. 2A–2D; abbreviations for brightness levels are found in the figure caption). The images were used to locate analysis points (Figs. 2A–2D). Imaging conditions maximized contrast between all zones in each sample; brightness levels do not correspond from sample to sample. Within

TABLE 1. Microprobe analyses of allanite and clinzoisite, Catalina amphibolite unit, Catalina Schist

No. anal.*	712841										41865										BCM			
	B					MM					41865					BCM								
	B	BG	G	DG	B	BG	G	MG	DG	VDG	B	BG	MG	DG	DGA	B	BG	G	DG	DG				
5	6	4	4	7	18/13	13/10	4	4	13/9	25/9	16/3	14/5	14/3	7/4	19/7	5/4	14/6	5						
33.8	34.4	34.9	36.2	36.5	37.1	37.4	37.7	38.8	39.6	34.0	35.3	37.1	37.4	38.1	35.9	36.4	37.4	37.4						
22.6	23.8	24.4	26.4	26.0	26.9	27.4	27.9	29.6	30.6	21.6	23.3	26.8	27.1	26.5	25.1	25.3	27.0	27.2						
0.13	0.11	0.10	0.07	0.06	0.06	0.06	0.05	0.03	0.02	0.85	0.66	0.42	0.40	0.15	0.16	0.24	0.18	0.14						
7.1	6.6	6.0	5.0	6.3	5.6	4.9	5.1	4.1	4.0	8.7	7.9	5.6	5.4	7.5	6.6	6.9	5.7	5.4						
1.5	1.3	1.1	0.73	0.65	0.59	0.84	0.47	0.31	0.13	0.40	0.60	0.30	0.30	0.10	0.71	0.53	0.45	0.40						
0.29	0.26	0.23	0.18	0.19	0.16	0.13	0.15	0.08	0.08	0.84	0.51	0.23	0.21	0.21	0.22	0.20	0.15	0.14						
14.7	15.9	16.9	19.5	18.6	19.5	19.8	20.4	22.5	23.9	14.9	17.7	20.7	21.1	23.8	18.2	19.4	21.0	21.6						
0.09	0.21	0.20	0.28	0.07	0.37	0.48	0.23	0.26	0.18	1.8	1.1	1.1	1.2	0.16	0.06	0.20	0.20	0.20						
4.4	3.2	2.8	1.6	2.0	1.6	1.6	1.2	0.82	0.03	3.0	1.8	0.70	0.60	0.02	2.0	1.5	1.1	1.0						
7.9	6.5	5.7	3.3	4.3	3.3	3.4	2.6	1.8	0.07	6.0	4.0	1.4	1.2	0.02	4.4	3.3	2.4	2.1						
0.25	0.30	0.28	0.23	0.26	0.22	0.22	0.20	0.17	0.03	0.32	0.27	0.20	0.16	0.02	0.29	0.26	0.21	0.20						
2.1	3.0	2.6	1.8	2.3	1.6	1.7	1.4	0.93	0.04	3.5	2.5	1.3	0.90	0.02	2.8	2.3	1.5	1.3						
0.24	0.61	0.52	0.43	0.54	0.34	0.37	0.33	0.21	0.01	0.89	0.68	0.53	0.30	0.01	0.78	0.70	0.41	0.35						
95.1§	96.2§	95.7§	95.7§	97.8	97.3	98.3	97.7	99.6	98.7	96.8	96.3	96.4	96.3	96.6	97.2	97.2	97.7	97.4						
14.9	13.6	11.9	7.4	9.4	7.1	7.3	5.7	3.9	0.18	13.7	9.3	4.1	3.16	0.09	10.3	8.1	5.6	5.0						
Formulae calculated on the basis of 12.5 O atoms																								
Si	2.99	2.98	2.99	3.00	3.01	3.02	3.01	3.00	3.01	3.00	3.00	3.01	3.01	3.00	3.00	3.00	3.00	3.00	3.00	3.00				
Al	2.36	2.43	2.47	2.58	2.53	2.60	2.64	2.70	2.74	2.25	2.33	2.56	2.57	2.46	2.48	2.46	2.56	2.57	2.57	2.57				
Cr	0.01	0.01	0.01	0.01	0.004	0.004	0.003	0.002	0.001	0.06	0.04	0.03	0.03	0.01	0.01	0.02	0.01	0.01	0.01	0.01				
Fe ^{3+***}	0.14	0.16	0.15	0.18	0.16	0.16	0.15	0.18	0.25	0.26	0.34	0.27	0.28	0.49	0.20	0.28	0.26	0.29	0.29	0.29				
Fe ^{2+***}	0.39	0.32	0.29	0.16	0.27	0.22	0.17	0.19	0.08	0.39	0.22	0.11	0.08	—	0.27	0.20	0.12	0.08	0.08	0.08				
Mg	0.20	0.17	0.14	0.09	0.08	0.07	0.10	0.06	0.04	0.02	0.05	0.08	0.04	0.01	0.09	0.07	0.05	0.05	0.05	0.05				
Zoct†	3.10	3.09	3.06	3.02	3.04	3.03	3.03	3.04	3.00	3.01	3.01	3.01	3.00	2.97	3.05	3.03	3.00	3.00	3.00	3.00				
Ca	1.40	1.47	1.55	1.73	1.64	1.70	1.71	1.75	1.94	1.41	1.61	1.80	1.82	2.01	1.63	1.72	1.81	1.85	1.85	1.85				
Mn	0.02	0.02	0.02	0.01	0.01	0.01	0.01	0.01	0.01	0.06	0.04	0.02	0.01	0.01	0.02	0.01	0.01	0.01	0.01	0.01				
Sr	0.01	0.01	0.01	0.01	0.003	0.02	0.02	0.01	0.01	0.09	0.06	0.05	0.06	0.01	0.003	0.01	0.01	0.01	0.01	0.01				
La	0.14	0.10	0.09	0.05	0.06	0.05	0.04	0.02	0.001	0.10	0.06	0.02	0.02	0.001	0.06	0.05	0.03	0.03	0.03	0.03				
Ce	0.26	0.21	0.18	0.10	0.13	0.10	0.08	0.05	0.002	0.19	0.12	0.04	0.03	0.001	0.14	0.10	0.07	0.06	0.06	0.06				
Pr**	0.01	0.01	0.01	0.01	0.01	0.01	0.01	0.005	0.001	0.01	0.01	0.01	0.01	0.01	0.01	0.01	0.01	0.01	0.01	0.01				
Nd	0.07	0.09	0.08	0.05	0.07	0.05	0.04	0.03	0.001	0.11	0.08	0.04	0.03	0.001	0.08	0.07	0.04	0.03	0.03	0.03				
Sm**	0.01	0.02	0.02	0.01	0.02	0.01	0.01	0.01	0.000	0.03	0.02	0.02	0.01	0.000	0.02	0.02	0.01	0.01	0.01	0.01				
Σ A‡	1.92	1.93	1.96	1.97	1.94	1.95	1.96	1.95	1.97	2.00	1.99	2.00	1.99	2.03	1.96	1.99	1.99	1.99	1.99	1.99				

Note: All data are in wt%. Abbreviations: B = bright; BG = bright gray; MG, G = gray; DG = dark gray; VDG = very dark gray; DGA = dark gray rims (see text).

** The second number, when present, indicates the number of points reanalyzed for Cr, Sr, and Mn.

† Estimated (see text).

‡ Al + Cr + Fe³⁺ + Fe²⁺ + Mg.

§ Ca + Mn + Sr + La + Ce + Pr + Nd + Sm.

¶ Does not include 0.6 wt% ThO₂ by microprobe.

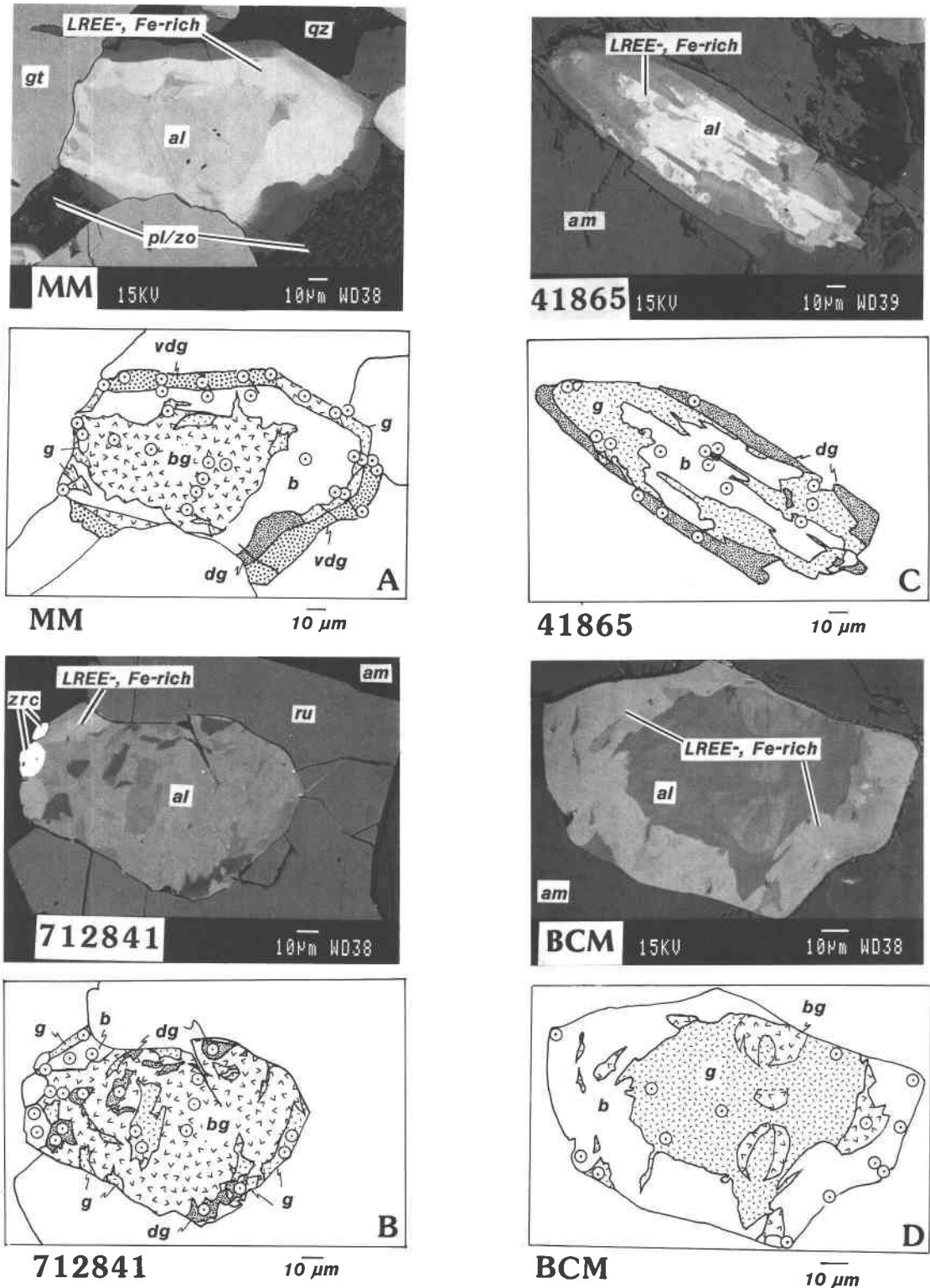


Fig. 2. Backscattered electron images (top) and maps of brightness zones (bottom) for samples MM (A), 712841 (B), 41865 (C), and BCM (D). Circles with dots represent locations of microprobe analyses. Mineral abbreviations are al = allanite, ap = apatite, pl = plagioclase, qz = quartz, zo = zoisite, zr = zircon. Other abbreviations are b = bright, bg = bright gray, g = gray, dg = dark gray, vdg = very dark gray. Darker patches in the bright core of 41865 (C, top) display fine-scale oscillatory zoning, which is poorly imaged at this magnification.

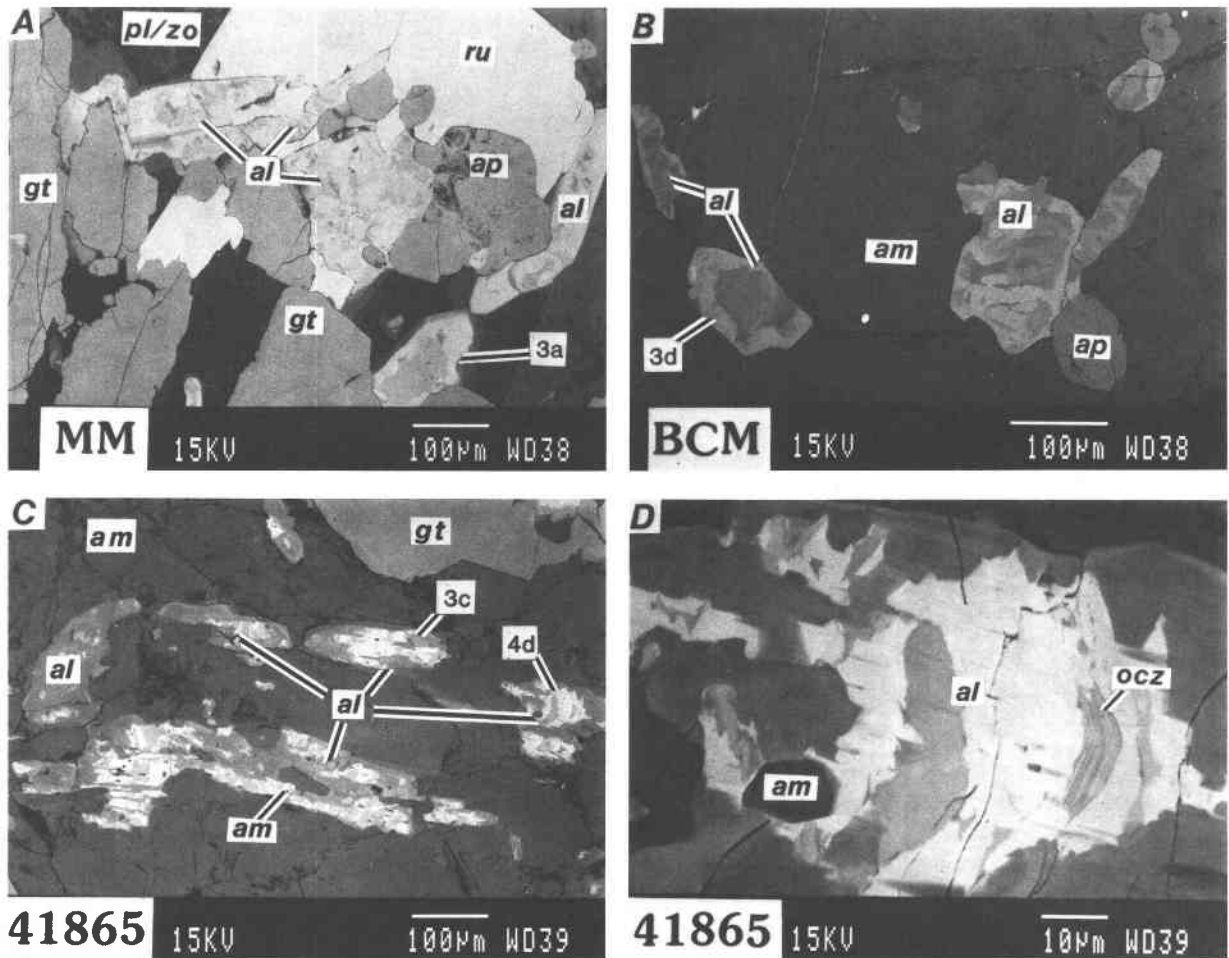


Fig. 3. Backscattered electron images of allanite from samples MM (A), BCM (B), 41865 (C, D). Abbreviations are as in Figure 2, with these additions: am = amphibole, gt = garnet, ru = rutile, ocz = region of oscillatory zoning. Grains shown at higher magnification in other figures are indicated by number-letter combinations.

individual samples, however (with one exception: the bg and g zones, sample MM, Table 1), the brighter the gray level, the higher the LREE content of the zone (Table 1). Within analytical uncertainties, zones of equal brightness in a single sample were of the same composition. Accordingly, in all but sample 712841 (in which only one grain was studied), several zones from different grains were analyzed, averaged, and reported in Table 1. Although dg zones are not present in the allanite grains from samples 41865 and BCM that are illustrated in Figures 2C and 2D, such zones are found in nearby grains (Fig. 3). The grains illustrated in Figure 2 are otherwise typical and representative of the thin section.

The accelerating voltage for the microprobe analyses was 15 kV, and the sample current was $\sim 0.025 \mu\text{A}$. Counting time for each point was 100 s. Standards for La, Ce, and Nd were pure synthetic phosphates of each element; the Th standard was an analyzed uraninite specimen (R11831) from the Roebling Collection (NMNH, Smithsonian Institution). Standards for other elements are listed in Sorensen (1988, Appendix II). Th was near or below

detection limits in these samples; data are reported only for sample 712841, which displayed a Th peak in wavelength scans.

The data for LREE were corrected for interelement interferences based on analyses of synthetic REE glasses (Drake and Weill, 1972). Backgrounds were measured on minerals comparable in Z to the allanite. Detection limits and interferences precluded analyses of Sm_2O_3 and Pr_2O_3 ; these elements are estimated by interpolation and extrapolation of the neighboring LREE in a chondrite-normalized REE pattern, as noted in Table 1.

Wavelength scans revealed minor amounts of Sr, Cr, and Mn, which were analyzed adjacent to spots analyzed for LREE and major elements. Ba, Ti, Y, and Na were not detected in wavelength scans. Relative errors are based on counting statistics for standards and samples; these errors are $\sim 1.2\%$ for Si, Al, Fe, Mg, and Ca, $\sim 10\text{--}20\%$ for Cr, Mn, and Sr, and $\sim 5\text{--}10\%$ for La, Ce, and Nd. The larger errors are associated with lower abundances of the minor elements and of LREE.

Formulae were calculated by normalizing to 12.5 O

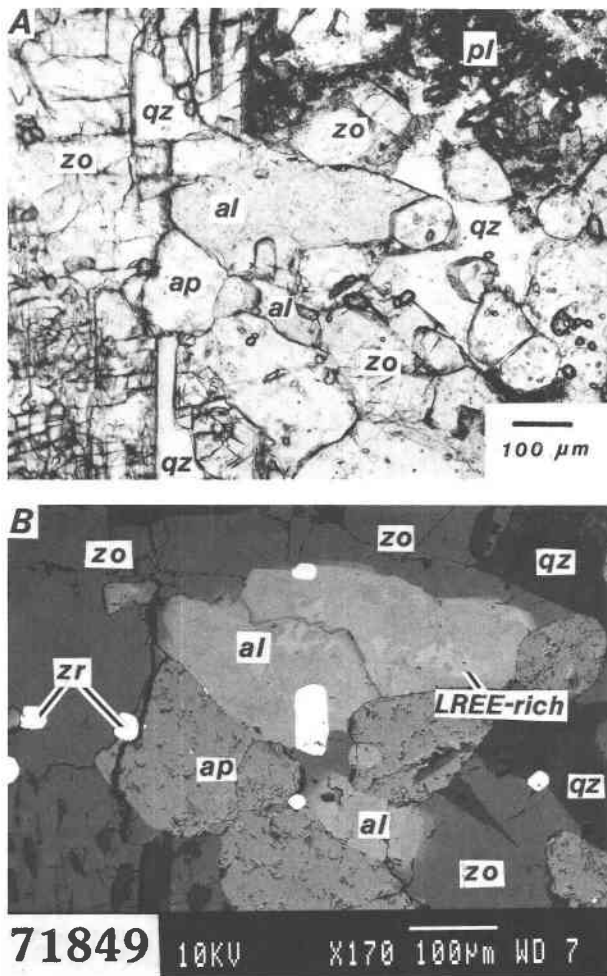


Fig. 4. Plane light (A) and backscattered electron images (B) of a leucocratic region (sample 71849) of a migmatitic block. Note the faint pleochroism of the allanitic core of the grain in the center of A, in contrast to colorless zoisite rims on allanite and overgrowths around apatite. Abbreviations are the same as in Figure 2.

atoms and 8 cations, which resulted in an estimate of $\text{Fe}^{2+}/\text{Fe}^{3+}$ ratios for all but two of the analyses reported in Table 1. Clinzoisite rims and replacement in samples MM and 41865 (vdg and dga; Table 1) were recalculated on the basis of $\text{Fe}_{\text{tot}} = \text{Fe}^{3+}$. Microprobe Fe values are reported as FeO.

RESULTS

Optical properties, zoning patterns, and textural relations

Optical properties. Unlike most allanite (Deer et al., 1986), the Catalina allanite samples are almost colorless. In plane light, they exhibit a faint tan to pinkish tan pleochroism compared to colorless rims and overgrowths of zoisite and clinzoisite (Fig. 4). Grain sizes range from approximately $10 \mu\text{m}$ to 0.5 mm (Figs. 3, 4). The Catalina allanite samples display low to upper first-order interfer-

ence colors. Anomalous interference colors were not observed, but grain extinctions are somewhat mottled. Only the prominent pleochroic halos in amphibole adjacent to allanite grains hint that the Catalina allanite samples are not clinzoisites. These optical properties are similar to those reported by Sakai et al. (1984) for what they termed REE-bearing epidote (total LREE to 15 wt% oxides) from chlorite- to oligoclase-biotite zone pelitic schists of the Sanbagawa subduction zone metamorphic terrane of central Shikoku, Japan.

Zoning. Although the zoning of the Catalina allanite is complex, in migmatites the LREE-richest composition is generally not found in grain cores. This apparent reverse zoning, in which an LREE-rich zone can be seen at grain margins or between core and rim, is illustrated in Figures 2 and 3. Sakai et al. (1984, their Fig. 5) depicted similar zoning patterns in the REE-bearing epidotes from the high-*P* metasedimentary rocks of the greenschist and amphibolite facies in the Sanbagawa terrane, which they interpreted as metamorphic features.

In the phengite-veined sample 41865, the zones with highest LREE contents are grain cores, and micrometer-scale oscillatory zoning and sectorlike features are developed between the compositions with highest contents of LREE (Figs. 2, 3). Tubular clusters of fluid inclusions, 5–15 μm long, bearing liquid + vapor are restricted to the cores of allanite from sample 41865. In samples MM and 41865, LREE-rich allanite is rimmed and replaced by zoisite, clinzoisite, or both (Figs. 2, 3; Table 1: compare analyses b and vdg, b and dga, respectively). Zoisite or clinzoisite rims or replacement features were not found in samples BCM or 712841.

Interpretation of textural relations. The relative timing of allanite crystallization in each of the four samples is based on inclusion relationships and other textural interpretations; this is summarized below.

In sample MM, allanite occurs as inclusions in garnet, amphibole, rutile, apatite, and plagioclase. Allanite in sample MM contains inclusions of zircon. In some large garnets in MM, inclusions of allanite occur in garnet growth zones that also contain inclusions of quartz and fluid inclusions 5–15 μm in diameter that have negative crystal shapes and contain liquid + vapor. Some of the quartz inclusions also contain fluid inclusions, 5–15 μm in diameter, bearing liquid + vapor. These relationships suggest that allanite was an early crystallizing mineral in sample MM and that fluids were present when grains of allanite and quartz were overgrown by garnet. However, allanite in MM also seems to have grown after garnet cracked and appears to have been somewhat corroded; in Figures 2A and 3A, the edge of a 3-mm garnet grain is cut by veinlets of the leucocratic assemblage plagioclase + quartz; this garnet is in contact with allanite, rutile, and saussuritized plagioclase. In Figure 3A, the large rutile grain contains inclusions of allanite, garnet, and apatite; the apatite grain also contains an inclusion of allanite. Allanite inclusions in apatite, rutile, garnet, and amphibole, as well as allanite grains in the matrix of melanocratic regions of the thin

section, lack the clinozoisite rims found where allanite is in contact with the plagioclase + quartz leucocratic assemblage (Figs. 3A, 4A).

In sample 712841, allanite occurs as inclusions in garnet, amphibole, and rutile, and contains inclusions of zircon. In Figure 2B, an allanite grain from sample 712841 occurs as an inclusion in a large rutile grain; the margin of the allanite grain that protrudes from the rutile is studied with two zircon grains. As in MM, allanite appears to have crystallized earlier than (or along with) garnet, amphibole, and rutile.

In sample BCM, allanite occurs as inclusions in garnet and amphibole, and contains inclusions of zircon. Garnet and amphibole (some with allanite inclusions) are themselves found as inclusions in saussuritized plagioclase of the leucocratic regions. As in the other migmatite samples, allanite in BCM appears to have crystallized earlier than (or along with) garnet and amphibole.

In nonmigmatitic sample 41865, allanite occurs as inclusions in amphibole, garnet, rutile, and phengite, and contains both fluid inclusions and inclusions of amphibole and zircon. The amphibole inclusions (Figs. 3C, 3D) show pleochroic haloes in plane light. Allanite inclusions found near the cores of garnets appear to lack the clinozoisite rims seen in matrix allanite. In this sample, which shows no evidence for partial melting, allanite appears to be an early crystallizing mineral which continued to crystallize along with amphibole.

Mineral chemistry

Catalina allanite displays a large range of Ca and LREE contents within single grains (Table 1; Fig. 5). The increases of LREE with $(\text{Fe}^{2+} + \text{Mg})$ and of $(\text{Ca} + \text{Sr} + \text{Mn})$ with $(\text{Al} + \text{Fe}^{3+} + \text{Cr})$, shown in Figure 5, are in general accord with the charge-coupled replacement of epidote or clinozoisite by REE: $\text{Ca}^{2+}(\text{Al,Fe})^{3+} \approx \text{REE}^{3+}\text{Fe}^{2+}$ (e.g., Deer et al., 1986; Peacor and Dunn, 1988). The Catalina allanite samples are Al rich and Fe poor. Al in the analyses of the Catalina allanite samples with the highest REE and Fe contents (Table 1) is greater than Al in the analyses of allanite reported in Deer et al. (1986), as well as that in all but three analyses of hydrothermal allanite reported by Exley (1980). Even allowing for the assumptions and inaccuracies of calculating $\text{Fe}^{2+}/\text{Fe}^{3+}$ based on microprobe analyses, the formulae for Catalina allanite all contain significantly more than two Al cations per 12.5 O atoms.

Minor amounts of Mg are present in Catalina allanite. Like Fe^{2+} , Mg^{2+} is an important charge balancing cation for REE³⁺ in these allanite samples; although the maximum Fe^{2+} contents of the allanite are approximately twice those of Mg, both increase regularly with LREE contents (Fig. 6). The role of Mg^{2+} in allanite chemistry was reemphasized by Peacor and Dunn (1988), who redefined magnesite orthite, naming it dollaseite-(Ce). Dollaseite-(Ce) is related to clinozoisite by the coupled substitution $\text{CaAl}_2\text{O} = \text{CeMg}_2\text{F}$ (Peacor and Dunn, 1988). Wavelength scans of the Catalina allanite samples did not reveal F. Grew et

al. (1989) reported a partial analysis of an allanite sample with $\text{MgO} > \text{FeO}$ from the eastern Sør Rondane Mountains, Antarctica. The analyses of Catalina allanite further document a significant $\text{Ca}^{2+}(\text{Al,Fe})^{3+} \approx \text{Mg}^{2+}\text{LREE}^{3+}$ exchange in allanite, most likely toward the fictive end-member $(\text{CaCe})(\text{MgAl}_2)\text{Si}_3\text{O}_{12}\text{OH}$ of Burt (1989).

LREE patterns of allanite zones

Chondrite-normalized LREE patterns of the brightness zones mapped in Figure 2 are plotted in Figure 7. In aggregate, the zones display LREE abundances ranging from approximately 10^4 to 10^5 times chondrite values (Fig. 7). Chondrite-normalized LREE abundances vary by factors of ~ 4 – 7 for samples 712841, MM, and BCM, and span almost an order of magnitude in sample 41865 (Fig. 7). Catalina allanite samples exhibit two general shapes of LREE patterns, straight and kinked (Fig. 7). Most zones from samples MM and 712841 have straight LREE patterns that decrease smoothly from La to Nd. In contrast, the zones from samples BCM and 41865 have kinked LREE patterns (Figs. 7C, 7D). The b zone of sample 712841 and the b and bg zones of sample 41865 differ in their LREE fractionation with respect to adjacent zones (Figs. 7A, 7C).

DISCUSSION

Evidence for hydrothermal allanite in the Catalina garnet amphibolites

In the Catalina amphibolite unit, allanite is found in metasomatized migmatitic and nonmigmatitic garnet amphibolite blocks. Allanite evidently crystallized prior to or along with garnet, amphibole, and rutile. Allanite grains in contact with saussuritized plagioclase in the leucocratic regions of migmatites display rims of clinozoisite or zoisite; those in melanocratic regions lack such rims. In the nonmigmatitic block 41865, allanite grains in the matrix display rims or replacement by clinozoisite or zoisite, whereas allanite grains that occur as inclusions in garnet generally do not.

If allanite crystallized prior to and along with amphibole and garnet, the mineral chemistry of the former two minerals and *P-T* estimates for the rocks suggest that allanite is probably not of igneous origin. In the migmatite samples, the compositions of garnet cores and rims fall within the range: almandine_{58–55} grossular_{15–34} pyrope_{26–09} spessartine_{02–03} (Sorensen, 1988). Amphiboles from migmatites are ferroan pargasite, ferroan pargasitic hornblende, and edenitic hornblende (Sorensen, 1988). The cores of garnets from migmatites have virtually identical compositions to counterparts in nonmigmatitic, less metasomatized, clinopyroxene-bearing blocks. The *P-T* conditions for metamorphism and migmatization of the unit ($T = 640$ – 750 °C, $P = 8$ – 11 kbar) are not compatible with crystallization of garnet and hornblende of these compositions from a melt. Allanite and garnet both contain fluid inclusions containing liquid + vapor. The fluid inclusions in garnet homogenize in the *T* range 136–169 °C; ice melts in the *T* range -2.0 to -0.7 °C, indicating

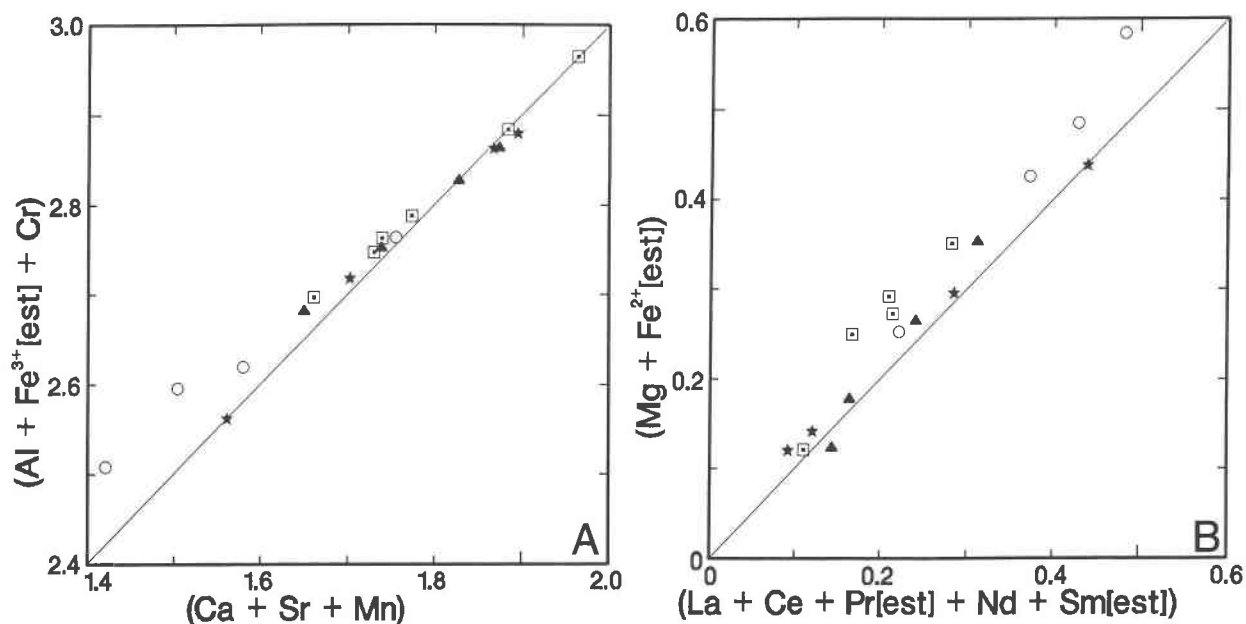


Fig. 5. Coupled substitutions in allanite. (A) M^{3+} vs. $(Ca + Sr + Mn)$; (B) LREE vs. $(Mg + Fe^{2+})$. Symbols as in Figure 1. The 1:1 line in A indicates components of chromian, strontian, or manganian epidote, zoisite, or clinozoisite; the 1:1 line in B represents an allanite component.

a low-salinity aqueous fluid (Sorensen and Barton, 1987). As is inferred for garnet and amphibole, the zoned allanite probably formed in a subsolidus fluid-rock regime, although some reequilibration of all of these minerals may have occurred during migmatization. Allanites and REE-rich epidote samples that are very similar in composition to Catalina allanite have been described from hydrothermally altered basalts (Exley, 1980) and from high P - T metasedimentary rocks (Sakai et al., 1984). In both of these cases, origin of the allanite or REE-rich epidote was ascribed to local subsolidus hydrothermal remobilization of LREE.

Cr, Sr, and Mn in Catalina allanite

Allanite from sample 41865 contains more Cr, Sr, and Mn than counterparts from migmatites (Table 1). The Cr_2O_3 contents of allanite from sample 41865, while considerably less than those of allanite from Outokumpu, Finland (Treloar and Charnley, 1987) are stoichiometrically significant (Table 1). Treloar and Charnley (1987) concluded that the chromian allanite in the metasedimentary rocks of Outokumpu reflected whole-rock enrichment of the protolith with Cr that was derived from an ultramafic and volcanic substrate.

The Cr_2O_3 contents of the allanite in 41865 increase with LREE (Table 1). Whole-rock sample 41865 is enriched in Cr compared to MORB, the clinopyroxene-bearing blocks, and the migmatites (Fig. 1). Although this block does not display a rind, its whole rock values for Cr and Ni resemble those of rind-bearing blocks and inner rinds reported by Sorensen and Grossman (1989). Like the rind-bearing blocks (Sorensen, 1988), this phengite-

veined block may have been contaminated by a component derived from metaultramafic rocks. If so, this metasomatism probably occurred while allanite was growing.

In allanite from migmatites, the zones richest in LREE are generally of lower Sr content (0.06–0.09 wt% SrO, b zones, Table 1) than zones slightly less rich in LREE (0.20–0.37 wt% SrO, bg zones, Table 1). In contrast, in sample 41865, the LREE-richest zone also contains the most Sr; all of the LREE-rich zones of allanite in this sample contain > 1 wt% SrO (Table 1). The b and bg zones of sample 41865 contain amounts of LREE comparable to the bg zone of sample 712841 and b zone of sample MM (Table 1). The former two zones contain 1.8 and 1.1 wt% SrO, respectively; the latter two contain 0.21 and 0.37 wt% SrO, respectively. The Sr contents of the Catalina allanite are probably not controlled by crystal-chemical effects related to LREE substitution. The presence of Sr-bearing (800–2000 $\mu\text{g/g}$; Sorensen and Grossman, 1989) plagioclase in the migmatites suggests that Sr enrichment is not likely to reflect the breakdown of an earlier Sr-rich mineral. Perhaps the Sr component in allanite was ultimately derived from metasomatic fluids that reacted with the Catalina garnet amphibolites. Brastad (1985) described extreme Sr enrichment in Ca-rich minerals (including epidote group minerals) in a metaeclogite from Norway, and attributed the enrichment to metasomatic introduction of Sr during amphibolitization.

In migmatites, the Mn content of allanite is low, and Mn is assumed to be Mn^{2+} . In the b and bg zones of sample 41865 (Table 1), reasonable cation proportions result from calculations that assume Mn^{2+} substitutes for Ca; poor formulae result from assuming that $Mn_{\text{tot}} = Mn^{3+}$.

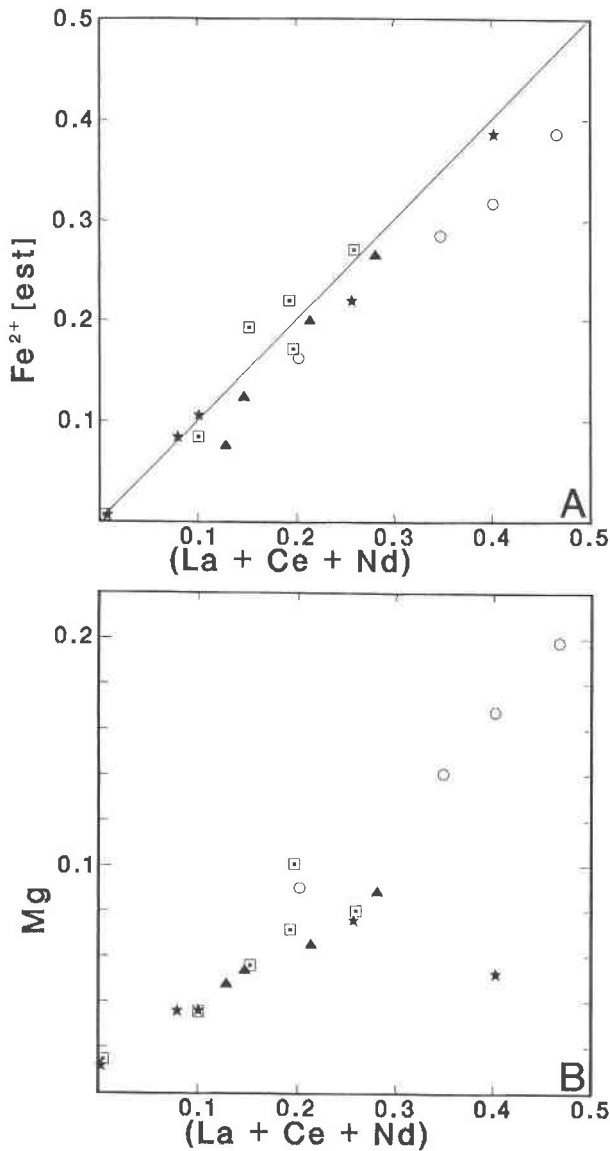


Fig. 6. LREE and M^{2+} cation substitutions in allanite. Symbols as in Figure 1. (A) LREE vs. estimated Fe^{2+} ; (B) LREE vs. Mg cations.

Possible origins of LREE zoning

Strong zoning of LREE is well documented for allanite from granitic rocks and for allanite formed in the hydrothermal systems generated by emplacement of granitic plutons (Exley, 1980; Gromet and Silver, 1983; Sawka et al., 1984). These studies report allanite cores that are richer in LREE than allanite rims. The authors attribute this normal zoning to crystallization of allanite from an evolving melt or late-stage fluid composition that is progressively depleted in LREE by, for example, decrease in bulk REE contents of the melt or changes in melt structure and thus partition coefficients. Such closed system models cannot easily account for the reverse zoning of allanite from the Catalina migmatites, which seems to indicate that

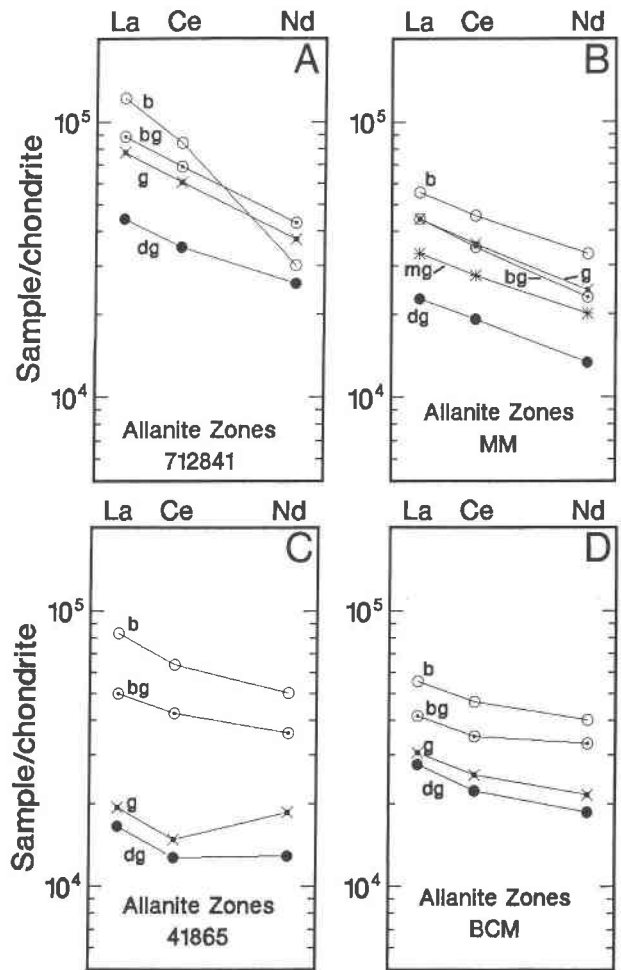


Fig. 7. LREE patterns of brightness zones in allanite samples from 712841 (A), MM (B), 41865 (C), and BCM (D). Normalization values for chondrite are from Anders and Ebihara (1982). Relative errors, based on counting statistics for REE standards (synthetic REE phosphates and the REE glasses of Drake and Weill, 1972) are ~5–10%. The larger errors are for abundances of LREE < ~2 wt%. Abbreviations are as in Figure 2, with the addition mg = medium gray (a gray level between g and dg, seen in some grains of sample MM). Symbols are circles with dots = bright zones, circles with dots = bright gray zones, squares with crosses = gray zones, asterisks = medium gray zones, and dg = dark gray zones.

LREE were added to the rock volume as the mineral grew.

The fine-scale oscillatory zoning observed in sample 41865 (Fig. 3) is beyond the limit of spatial resolution for microprobe analysis. Scanning electron microscopy and energy-dispersive analysis suggest that the oscillatory zoning represents alternating LREE-richer and LREE-poorer compositions. Gromet and Silver (1983) observed sharp euhedral oscillatory-zoned bands in a few allanite grains in a granodiorite from the northeastern margin of the Peninsular Ranges of southern California, which they interpreted as evidence for origin by growth from a melt. The lack of evidence for partial melting of sample 41865

and the oscillatory zoning of its allanite suggests that subsolidus growth of allanite may also produce oscillatory zoning.

The textures and LREE zoning of the Catalina allanite suggest that the overall process of trace element enrichment changed with time. The distributions of LREE within allanite from samples BCM, MM, and 712841 indicate that the LREE-richest compositions did not form during the earliest stages of allanite crystallization (Figs. 2, 3; Table 1). The partial replacement of b cores of grains in sample 41865 with less LREE-rich compositions suggests that allanite (Figs. 2, 3; Table 1) was destabilized and partially dissolved in a regime that was still capable of saturating allanite. Late-stage zoisite or clinozoisite, or both, formed as rims on and replacement of LREE-rich compositions in two of the four samples studied. These textures indicate that allanite was a highly reactive mineral. Because the bulk composition of allanite controls that of individual blocks (compare Figs. 1 and 7), the large differences in the LREE compositions of enriched blocks suggest that there were local, time-dependent heterogeneities or variations, or both, in the geochemical enrichment process that affected the garnet amphibolites.

Allanite from nonmigmatitic block 41865 has significant amounts of Sr and Cr, and displays normal zoning of LREE. Metamorphic textures indicate that allanite crystallized prior to formation of phengite veins in the block. The composition of the phengite and the whole-rock chemistry of sample 41865 suggest that the veining event reflects high-*P*, moderate- to high-*T* alkali metasomatism. If, as seems likely, the allanite is a metasomatic mineral, the fluids from which it crystallized, or with which it equilibrated, may have carried a Cr-rich component derived from the metamorphosed ultramafic matrix of the block, as well as a Sr + LREE component. If the latter component is of exotic origin, then this rock was first altered by exchange with metaultramafic rocks and a fluid enriched in Sr + LREE that produced the zoned allanite and was subsequently metasomatized by alkali-rich fluids that deposited phengite in veins.

The decoupling of Sr and LREE enrichment and the reverse zoning of allanites in migmatites suggest that the processes that affected sample 41865 differed from those that enriched the migmatites. If, for example, the infiltration of an Sr + LREE-rich fluid initiated melting, the reverse zoning and lack of Sr enrichment of the allanite from migmatites might reflect cocrystallization of the REE-rich zones of allanite and plagioclase in an open system melting process. Sorensen and Grossman (1989) found that apatite and sphene from migmatite sample MM were depleted in LREE and enriched in middle REE compared to counterparts from nonmigmatitic blocks. Perhaps allanite, apatite, sphene, and plagioclase all equilibrated with each other in the presence of a fluid or melt.

By analogy with the interpretations of changes in REE patterns in zoned igneous allanite, it seems possible that the LREE zoning and the different shaped LREE patterns of the Catalina allanite reflect time-dependent changes in

the bulk LREE contents and fractionations of the metasomatic agent(s) between different samples. These changes could represent more than one source for introduced LREE (e.g., fluids derived from subducted sediment vs. fluids derived from the subducted slab), different media of LREE transport (fluids vs. melts), or compositional evolution of fluid or melt along reactive flow paths. Whether LREE were deposited from fluids or melts, the diameters of blocks and the size of the complex as a whole indicate that the metasomatic agent(s) had heterogeneous effects on a scale of several meters to kilometers.

On a much finer scale (and for more elements), similar conclusions were reached by Philippot and Selverstone (1989a, 1989b). These authors explained a diverse suite of Ba-, K-, HFSE-, and LREE-bearing daughter minerals in fluid inclusions in veins of omphacite from eclogites in the western Alps to reflect millimeter-scale compositional heterogeneities in metamorphic fluids. A somewhat similar conclusion was reached by Sakai et al. (1984) in their study of REE-bearing epidote from pelitic schists of the high *P-T* Sanbagawa metamorphic terrane of Japan. Citing the strong preferred orientation of REE-bearing epidote, an increase in this mineral's average grain size with metamorphic grade, and an increase in the volume of REE-rich overgrowths upon REE-poor or REE-free epidote with metamorphic grade, these authors concluded that reverse zoned REE-bearing epidote in the Sanbagawa pelitic schists was of metamorphic origin. Sakai et al. (1984) also found orange to brown, Fe-rich, Ca-poor allanite rimmed by REE-bearing and REE-free epidote in the Sanbagawa pelitic schists. Based on the constant grain size of the allanite in both low- and high-grade rocks, its irregular, anhedral shape, and its chemical composition, the allanite was interpreted to be of detrital origin (Sakai et al., 1984). These authors suggested that the REE-bearing epidote was deposited from fluids that had partially dissolved detrital allanite and locally redeposited a less REE-rich epidote. The process was thought to have ceased once rims of REE-bearing or REE-free epidote armored the detrital allanite grains.

This study, the work of Philippot and Selverstone (1989a, 1989b), and the results of Sakai et al. (1984) suggest that the element transport properties of fluids in subduction zone metamorphic environments, although considerable, may be heterogeneous on a scale of millimeters to kilometers. As was pointed out by Franz et al. (1989), the length scales of fluid-rock interaction in high *P-T* terranes must be better understood in order to evaluate the importance of fluids as metasomatic agents in deep regions of convergent margins.

CONCLUSIONS

Allanite from the Catalina mafic and ultramafic complex displays zoning of LREE that may in part reflect changes in fluid compositions in the metasomatic-hydrothermal system in which it formed. Variations of Ca, LREE, Al, Cr, Sr, Fe, Mg, and Mn within zoned grains indicate a fairly continuous nature for many substitutions

of M^{2+} and M^{3+} cations in allanite. LREE (and perhaps Cr and Sr) may have been transported by hydrothermal fluids, or by melts generated by fluid infiltration, on a scale of several meters to kilometers in the Catalina mafic and ultramafic complex.

ACKNOWLEDGMENTS

I thank E. Jarosewich, J. Nelen, J. Collins, G. MacPherson, and E. O'Leary for help with the analyses and in preparation of the figures. I thank the Santa Catalina Island Conservancy, particularly D. Propst and T. Martin, for permission and logistics for the field work. The research was supported by the Sprague and Becker Funds of the Smithsonian Institution. Discussions with J.N. Grossman, W.A. Dollase, and P.J. Dunn are gratefully acknowledged. An early version of this paper was reviewed by W.A. Dollase, P.J. Heaney, D.D. Hickmott, J. Philpotts, W.M. Thomas, and M. Wise. S.M. Peacock and an anonymous person reviewed the submitted version of the manuscript.

REFERENCES CITED

- Anders, E.A., and Ebihara, M. (1982) Solar-system abundances of the elements. *Geochimica et Cosmochimica Acta*, 46, 2363–2380.
- Anderson, R.N., Delong, S.E., and Schwarz, W.M. (1976) Thermal model for subduction with dehydration in the downgoing slab. *Journal of Geology*, 86, 731–739.
- Anderson, R.N., Uyeda, S., and Miyashiro, A. (1978) Geophysical and geochemical constraints at converging plate boundaries—Part I: Dehydration in the downgoing slab. *Geophysical Journal of the Royal Astronomical Society*, 44, 333–357.
- Bebout, G.E., and Barton, M.D. (1989) Fluid flow and metasomatism in a subduction zone hydrothermal system: Catalina Schist terrane, California. *Geology*, 17, 976–980.
- Bertasi, R.P., and Barton, M.D. (1989) Phase equilibria of a high-pressure melange pegmatite: Implications for partial melting and volatile transfer during subduction. *Eos*, 70, 1376.
- Boulégue, J., Iiyama, J.T., Charlou, J.-L., and Jedwab, J. (1987) Nankai Trough, Japan Trench, and Kuril Trench: Geochemistry of fluids sampled by submersible "Nautile." *Earth and Planetary Science Letters*, 83, 363–375.
- Brastad, K. (1985) Sr metasomatism, and partition of Sr between mineral phases of a meta-eclogite from Bjorkedal, West Norway. *Tschermaks Mineralogische und Petrographische Mitteilungen*, 34, 87–103.
- Burt, D.L. (1989) Compositional and phase relations among rare earth element minerals. In *Mineralogical Society of America Reviews in Mineralogy*, 21, 259–302.
- Coleman, R.G. (1961) Jadeite deposits of the Clear Creek area, New Idria District, San Benito County, California. *Journal of Petrology*, 2, 209–247.
- (1967) Low-temperature reaction zones and alpine ultramafic rocks of California, Oregon, and Washington. *United States Geological Survey Bulletin* 1247, 1–49.
- Curtis, C.D., and Brown, P.E. (1969) The metasomatic development of the zoned ultrabasic bodies of Unst, Scotland. *Contributions to Mineralogy and Petrology*, 24, 275–292.
- (1971) Trace element behavior in the zoned metasomatic bodies of Unst, Scotland. *Contributions to Mineralogy and Petrology* 31, 87–93.
- Deer, W.A., Howie, R.A., and Zussman, J. (1986) Epidote group. In *Rock-forming minerals*, vol. 1B: Disilicates and ring silicates (2nd edition), p. 2–151. Longman, London.
- Delany, J.M., and Helgeson, H.C. (1978) Calculation of the thermodynamic consequences of dehydration in subducting oceanic crust to 100 kb and >800 °C. *American Journal of Science*, 278, 638–686.
- Drake, M.D., and Weill, D.F. (1972) New rare earth element standards for electron microprobe analysis. *Chemical Geology*, 10, 179–181.
- Exley, R.A. (1980) Microprobe studies of REE-rich accessory minerals: Implications for Skye granite petrogenesis and REE mobility in hydrothermal systems. *Earth and Planetary Science Letters*, 48, 97–110.
- Franz, G., Thomas, S., and Selverstone, J. (1989) Fluids in eclogites: Evidence from high-pressure veins in the Austrian Alps. *Eos*, 70, 1377.
- Grew, E.S., Asami, M., and Makimoto, H. (1989) Preliminary petrological studies of the metamorphic rocks of the eastern Sør Rondane Mountains. *Proceedings NIPR Symposium on Antarctic Geosciences*, 3, 100–127.
- Gromet, L.P., and Silver, L.T. (1983) Rare earth element distributions among minerals in a granodiorite and their petrogenetic implications. *Geochimica et Cosmochimica Acta*, 47, 925–939.
- Mattinson, J.M. (1986) Geochronology of high-pressure-low-temperature Franciscan metabasites: A new approach using the U-Pb system. *Geological Society of America Memoir* 164, 95–105.
- Moore, D.E. (1984) Metamorphic history of a high-grade blueschist exotic block from the Franciscan Complex, California. *Journal of Petrology*, 25, 126–150.
- Peacock, S.M. (1987a) Creation and preservation of subduction-related metamorphic gradients. *Journal of Geophysical Research*, 92, 12763–12781.
- (1987b) Thermal effects of metamorphic fluids in subduction zones. *Geology*, 15, 1057–1060.
- Peacor, D.R., and Dunn, P.J. (1988) Dollaseite-(Ce) (magnesium orthite redefined): Structural refinement and implications for F + M²⁺ substitutions in epidote-group minerals. *American Mineralogist*, 73, 838–842.
- Pearce, J.A. (1982) Trace element characteristics of lavas from destructive plate boundaries. In R.S. Thorpe, Ed., *Andesites*, p. 525–548. Wiley, New York.
- Philippot, P., and Selverstone, J. (1989a) Fluid inclusions in eclogite veins: Evidence for fluid heterogeneities and high-field-strength element mobility. *Geological Society of America Abstracts with Programs*, 21, A359.
- (1989b) Fluid heterogeneities, migration pulses, and channelized flow of eclogite facies fluids: Evidence for Zr, Ti, Ba, and K mobility in subduction zones. *Eos*, 70, 1377.
- Platt, J. P. (1975) Metamorphic and deformational processes in the Franciscan Complex, California: Some insights from the Catalina Schist terrain. *Geological Society of America Bulletin*, 86, 1337–1347.
- (1976) The petrology, structure, and geologic history of the Catalina Schist terrain, southern California. *University of California Publications in the Geological Sciences*, 112, 1–111.
- Reck, B.H. (1987) Implications of measured thermal gradients for water movement through the northeast Japan accretionary prism. *Journal of Geophysical Research*, 92, 3683–3690.
- Sakai, C., Higashino, T., and Enami, M. (1984) REE-bearing epidote from Sanbagawa pelitic schists, central Shikoku, Japan. *Geochemical Journal*, 18, 45–53.
- Sanford, R.F. (1982) Growth of ultramafic reaction zones in greenschist to amphibolite facies metamorphism. *American Journal of Science*, 282, 344–360.
- Sawka, W.N. (1988) REE and trace element variations in accessory minerals and hornblende from the strongly zoned McMurphy Meadows Pluton, California. *Transactions of the Royal Society of Edinburgh: Earth Sciences*, 79, 157–168.
- Sawka, W.N., Chappel, B.W., and Norrish, K. (1984) Light-rare-earth-element zoning in sphene and allanite during granitoid fractionation. *Geology*, 12, 131–134.
- Sorensen, S.S. (1988) Petrology of amphibolite-facies mafic and ultramafic rocks from the Catalina Schist, southern California: Metasomatism and migmatization in a subduction zone metamorphic setting. *Journal of Metamorphic Geology*, 6, 405–435.
- (1989) Trace element metasomatic effects of the initiation of subduction? Catalina Schist, southern California. *Geological Society of America Abstracts with Programs*, 21, A216.
- Sorensen, S.S., and Barton, M.D. (1987) Metasomatism and partial melting in a subduction complex: Catalina Schist, southern California. *Geology*, 15, 115–118.
- Sorensen, S.S., and Grossman, J.N. (1989) Enrichment of trace elements in garnet amphibolites from a paleo-subduction zone: Catalina Schist, southern California. *Geochimica et Cosmochimica Acta*, 53, 3155–3177.
- Suppe, J., and Armstrong, R.L. (1972) Potassium-argon dating of Franciscan metamorphic rocks. *American Journal of Science*, 272, 217–233.
- Treloar, P.J., and Charnley, N.R. (1987) Chromian allanite from Outokumpu, Finland. *Canadian Mineralogist*, 25, 413–418.

APPENDIX TABLE I. Analyses of garnet amphibolite blocks containing veins of phengite

	41865	41866	7484SC3		41865	41866	7484SC3
SiO ₂ (%)	40.7	45.0	40.1	Rb (ppm)	28.7	25.9	45
TiO ₂	3.7	1.91	5.3	Sr	74	106	152
Al ₂ O ₃	17.6	14.9	16.2	Y	75	60	71
FeO	17.7	16.3	14.2	Zr	191	218	430
MnO	0.73	0.36	0.22	Nb	32	11	81
MgO	7.6	8.6	6.9	Cs	0.47	0.49	0.44
CaO	9.3	9.6	11.7	Ba	590	300	840
Na ₂ O	0.66	0.91	0.53	La	31	25	45
K ₂ O	0.88	1.00	1.77	Ce	62	53	90
P ₂ O ₅	<0.05	<0.05	1.91	Nd	43	34	47
LOI	1.24	1.24	1.55	Sm	12.1	12.0	11.8
Σ	100.1	99.8	100.4	Eu	3.9	3.7	4.9
				Tb	1.66	1.86	1.80
Sc (ppm)	64	49	37	Yb	6.9	6.2	4.8
Cr	650	380	69	Lu	0.97	0.88	0.64
Co	60	48	35	Hf	4.8	6.4	9.8
Ni	198	157	89	Ta	2.03	0.63	5.9
Cu	21	24	20	Th	2.97	6.2	4.9
Zn	93	141	71	U	1.37	2.54	3.2

Note: Abbreviations: LOI = loss on ignition. Analyses done by INAA and XRF using method of Sorensen and Grossman (1989).